Influence of oscillatory centrifugal forces on the mechanism of Turing pattern formation

Jacobo Guiu-Souto* and Alberto P. Muñuzuri

Group of Nonlinear Physics, Department of Physics, University of Santiago de Compostela, E-15782 Santiago de Compostela, Spain

(Received 29 April 2014; published 21 January 2015)

Constantly acting centrifugal forces on Turing pattern forming systems have been observed to induce orientation and wavelength changes on Turing structures. Here, we will consider a periodic modulation of such centrifugal forces and their effects on pattern formation. Depending on the oscillation period the system exhibits a wide variety of stationary (stripes, H_0, etc.) or nonstationary patterns (black eyes, etc.), as well as transitions and instabilities such as Eckhaus, zigzag, etc. In this paper, a detailed description of the different patterns and patterning mechanisms will be described and understood within the previous context. The system considered is the Belousov-Zhabotinsky reaction encapsulated in AOT micelles modeled by the adapted version of the Oregonator model.

DOI: 10.1103/PhysRevE.91.012917 PACS number(s): 05.45.−a, 87.18.Hf, 82.33.Nq, 47.54.−r

I. INTRODUCTION

Recent studies have revealed that Turing pattern formation is highly sensitive to external forcings modifying its diffusive transport and reaction kinetics [1–5]. The Turing mechanism [6,7] is commonly used to model and understand symmetry breaking processes [8–11] that occur in nature, as patterns on animal coats and fish skin [12,13] or mammalian brain labyrinthine patterns [14]. Nevertheless, the disparities of the diffusion processes involved in the Turing mechanism make it difficult to be obtained in controlled experiments [15]. In addition, in biology, this type of pattern is usually developed under the influence of external factors in its environment that actually control the final arrangement of the pattern [16–18].

In this regard, studies on Turing instability under an external controlled forcing, as, for example, temperature gradients, concentration constraints, and luminous moving boundaries, have allowed improving our knowledge about the complex mechanisms involved in pattern formation phenomena [19–21]. Likewise, it provides a tool to test the nonlinear character of pattern formation under nonequilibrium constraints. Depending on the system parameters, Turing instability is expressed by means of different spatial configurations ranging from spots of oxidized catalyst with a hexagonal arrangement (H_0) or spots of reduced catalyst with hexagonal configuration on an oxidized background (H_π) to completely disorganized labyrinthine configuration [22,23]. Furthermore, for certain regimes of the external perturbation the system can exhibit reversed patterns (when the pattern and its background exchange their colors). This is the case of the well-known honey combs or black spots patterns [24]. Along the reorganization processes, long-wave instabilities [25,26] may occur (i.e., zigzag or Eckhaus instabilities). These instabilities appear when the system undergoes an alteration on its characteristic wavelength and the pattern tries to adapt to the current configuration.

Here we present a numerical study for quasi-two-dimensional Turing pattern formation subjected to an oscillating centrifugal force. Turing instability is modeled by the Oregonator-like set of equations [27] that takes into account the main properties of the water-in-oil Belousov-Zhabotinsky–aerosol-OT (BZ-AOT) microemulsion system [28–31]. This is a micellar medium in which the BZ aqueous reaction [28,29] is surrounded by the AOT surfactant forming nanodroplets, and these droplets are immersed in the oil phase. It may be considered as a closed encapsulated system where only diffusive transport is allowed [4]. This configuration allows introducing important differences in the diffusive transport of the main chemical species of the system that are responsible for Turing pattern formation [6].

A previous work [32] has already shown, both numerically and experimentally, that Turing patterns in BZ-AOT medium under the effect of a constant centrifugal force may experience important changes in the diffusion mechanisms. In particular, the intensity of the external forcing directly affects the diffusion coefficients of both species, the effect being modulated by the molecular weight of each species. This effect is immediately translated into a modification of the characteristics of the Turing pattern (wavelength, orientation, etc.) that for large forcings results in a complete suppression of the patterns.

The goal of this paper is to analyze the effect of a centrifugal force on such a system when its amplitude is periodically modulated with time. Especially interesting will be the case when the modulation period of the external forcing is comparable with a characteristic time of the system. For the present case and following an experimentally inspired approach, we choose as characteristic time the time required by a pattern in absence of any forcing to develop. A similar approach, in a different context, was performed by [33,34] in the chlorine dioxine-iodine-malonic acid (CDIMA) reaction in an open system subjected to a luminous moving forcing. Depending on the velocity of the forcing, Turing patterns presented different spatial arrangements: parallel, oblique, and perpendicular [33].

The outline of the paper is as follows. In Sec. II, we present the reaction-diffusion model equations, and describe both the computational domain and the numerical techniques. The results of the simulations are shown in Sec. III. Firstly, we analyze the effect of the modulation in the centrifugal force far from the rotation center in order to avoid the radial dependence and obtain homogeneous patterns. Then by an analysis close to the center we consider the effect of a gradient in the anisotropy

*Present address: University Hospital of Santiago de Compostela, E-15706 Santiago de Compostela, Spain.

induced in the system. The paper ends with the conclusions and discussion of the results in Sec. IV.

II. MODEL

The BZ-AOT system involves a complex set of chemical reactions [30,35]. However, the mechanism of Turing pattern formation in such a system has been successfully modeled by the two-variable modified Oregonator model [24,27]:

$$\varepsilon\frac{\partial c_1}{\partial t} = fc_2\frac{q-c_1}{q+c_1} + c_1\frac{1-\mu c_2}{1-\mu c_2+\varepsilon_1} - c_1^2 + \nabla\cdot(D_1\nabla c_1), \tag{1}$$

$$\frac{\partial c_2}{\partial t} = c_1\frac{1-\mu c_2}{1-\mu c_2+\varepsilon_1} - c_2 + \nabla\cdot(D_2\nabla c_2), \tag{2}$$

where c_i represents the dimensionless concentrations of the activator ($i = 1$) and inhibitor ($i = 2$) species. The parameters f, μ, q, ε, and ε_1 depend on the reaction rates and they appear as a result of applying the mass action law on the chemical equations [24]. D_1^0 and D_2^0 are the diffusion coefficients for both relevant species in absence of any external influence. The suitable values to get Turing patterns (through a supercritical Turing instability) in this model[1] are $f = 1.2$, $\mu = 190$, $q = 0.001$, $\varepsilon_1 = 0.01$, $\varepsilon = 0.8$, $D_1^0 = 1\,\text{s.u.}^2/\text{t.u.}$, and $D_2^0 = 100\,\text{s.u.}^2/\text{t.u.}$ as used throughout this study [24].

The effect of a centrifugal force on this system has been previously modeled [32,36] by introducing a radial-dependent diffusion coefficient as follows:

$$D_{1,2}(\beta,m_{1,2},R,t) = \frac{D^0_{1,2}(\beta,m_{1,2})}{3\sqrt{3}}[3+2\Phi_{1,2}(\beta,m,\omega(t),R)]^{3/2}, \tag{3}$$

with

$$\Phi_{1,2}(\beta,m_{1,2},\omega(t),R) = \tfrac{1}{2}\beta m_{1,2}\omega^2(t)R^2, \tag{4}$$

where $m_{1,2}$ are the masses of both species, ω the angular velocity, $D^0_{1,2}(\beta,m_{1,2})$ are the diffusion coefficients in absence of forcing (as stated before), and $\beta = 1/k_B\Theta$ with Θ as the absolute temperature. $\Phi_{1,2}(\beta, m, \omega(t), R)$ is a dimensionless function that takes into account the magnitude of the centrifugal forcing. Note that now the diffusion coefficients explicitly depend on the distance to the rotation center (given by R). Note that the effect of the forcing on the diffusion coefficients is multiplied by the molecular weight [Eq. (4)]; thus for large forcings the heaviest species is expected to diffuse faster than the lightest and the Turing mechanism conditions might be violated [32]. As the diffusion coefficient depends explicitly on R, this mathematically introduces some convective terms in the equations that are going to be responsible for some of the dynamics described below. In particular, the most probable wavelength of the Turing structures in the system is now explicitly dependent on the intensity of the external forcing [given by $\omega(t)\,R$] as calculated in [32]. The expression is rather complicated but as a first-order approximation it looks this way [32]:

$$\Delta\lambda = \frac{\lambda}{\lambda_0} - 1 \propto [\omega(t)R]^2, \tag{5}$$

where $\Delta\lambda$ stands for the wavelength variations of the forced pattern with respect to the standard pattern, with λ and λ_0 being their respective wavelengths. Note that this is the most probable value of the wavelength although other values are also possible even if they are not the most probable [10,32].

Here we consider that the rotational angular velocity, given by $\omega(t)$, is periodically modulated following

$$\omega(t) = \frac{\omega_0}{2}\left[1-\cos\left(\frac{2\pi}{T}t\right)\right], \tag{6}$$

where ω_0 is the maximum rotation velocity and T represents the period of modulation of the centrifugal force. These will be our control parameters in the following.

Numerical simulations of Eqs. (1) and (2) are performed by applying an explicit three-level in time, and centered in space, integration scheme (Du Fort–Frankel scheme) [37] with a spatial step of 0.2 s.u., a time step of 10^{-3} t.u. and zero flux boundary conditions. The computational domain is constituted by a square mesh of 300×300 grid points. The period of the forcing T is varied around the characteristic time of the system, $\tau = 600$ t.u., i.e., the time needed by the system to develop the pattern; it is an indirect measurement of the reacting time upon external perturbations. To trigger the instability we use random noise as an initial condition.

III. RESULTS

In our analysis the three control parameters used to modify the centrifugal force are the maximum rotation frequency (ω_0), the period of the modulation of the rotation frequency (T), and the distance to the rotation center (R). Firstly, the effect of T will be analyzed when observations are performed far from the rotational center (keeping constant $\omega_0 = 0.025\,\text{rad/t.u.}$ and $R = 1000\,\text{s.u.}$) Secondly, both the effect of T and a strong gradient on the centrifugal force will be studied in the vicinity of the rotation center with the maximum rotation frequency fixed at 0.4 rad/t.u.

At the limiting case of $T \ll \tau$, the centrifugal force is practically constant; therefore depending on its magnitude the system exhibits different configurations ranging from stripes to complete suppression of the patterns. For intermediate values the system may exhibit hexagons (H_0, H_π) or mixed states as described in [32].

A. Effect of periodicity of the centrifugal forcing, T

For the simulations presented here, we always considered an integration domain located far from the rotational center (radius equal to 1000 s.u.) in order to avoid gradients in the system; thus the centrifugal force along the domain keeps its direction constant and it basically depends on T. For the particular figures in this paper the direction of the centrifugal force was chosen along the diagonal of the third quadrant. ω_0 was kept constant ($\omega_0 = 0.025\,\text{rad/t.u.}$) for the simulations in this subsection. This value of ω_0, if kept constant [32], is able

[1] s.u. and t.u. denote spatial/temporal dimensionless units from the scaled numerical model [24].

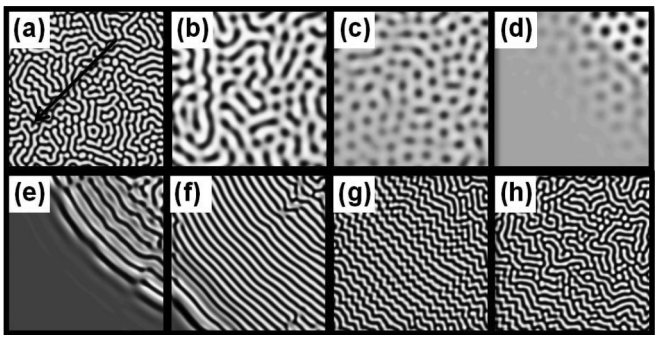

FIG. 1. Effect of the oscillating forcing $\omega(t)$ on Turing pattern formation along a full oscillation for $T \sim \tau$. (a–h) correspond to $\omega(t)/\omega_0$: 0, 0.6, 0.7, 1.0, 0.8, 0.6, 0.3, and 0, respectively. The direction of the oscillatory force is fixed along the diagonal of the third quadrant [see arrow in (a)] with a maximum value fixed in $\omega_0 = 0.025$ rad/t.u.

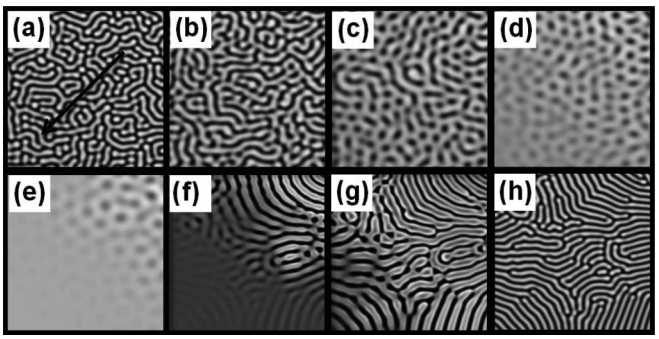

FIG. 2. Effect of the oscillating forcing $\omega(t)$ on Turing pattern formation along a full oscillation for $T \sim 10\tau$. (a–h) correspond to $\omega(t)/\omega_0$: 0, 0.5, 0.7, 0.8, 1, 0.7, 0.5, and 0.2, respectively. The direction of the oscillatory force is fixed along the diagonal of the third quadrant [see arrow in (a)] with a maximum value fixed in $\omega_0 = 0.025$ rad/t.u.

to suppress completely the pattern, the effect being stronger in the lower right corner of each picture.

Very low values of T ($T \ll \tau$) result in the formation of a steady pattern in the domain, that corresponds to the average value of $\langle\omega(t)\rangle$, a mixed state of spots and stripes. In this case, the patterns tend to align along the direction of the centrifugal force as in Ref. [32].

As T is increased, the modulation period becomes comparable with the characteristic time in the system (τ) and nontrivial behaviors are expected. For $T \sim \tau$, the system exhibits a complicated dynamic that periodically repeats along time as $\omega(t)$ varies. The different snapshots in Fig. 1 present the evolution of the pattern along a complete oscillation of $\omega(t)$. At the beginning of the cycle [$\omega(t) = 0$] the system exhibits a standard pattern (the one that could be observed in absence of external forcing). As $\omega(t)$ increases the pattern tries to adapt to the new value changing its configuration into inverted stripes and H_π until it is completely suppressed at $\omega(t) \sim \omega_0$. Note that in the corresponding snapshot not the whole domain is homogeneous as the centrifugal force is slightly smaller in the areas where the radius is slightly smaller (upper right corner of the figure) and some remaining of the pattern can still be observed. As time increases, $\omega(t)$ decreases and the area covered by the pattern grows. Now the pattern clearly exhibits a stripe geometry with stripes oriented in the direction perpendicular to the centrifugal forcing [see Fig. 1(e)]. It is noteworthy to observe the evolution to reach this configuration of perpendicular stripes. In fact, not only the type of pattern changes with time as the forcing decreases but also the wavelength of the pattern is modified, becoming smaller. In Figs. 1(b) and 1(c) the wavelength that the system is able to support is larger than in Figs. 1(d) and 1(e), thus, as time goes on, the pattern exhibited needs to readjust to the new wavelength and this is done through the splitting of the existing stripes, as is clearly seen in Fig. 1(e) [26,38]. After the situation shown in Fig. 1(f), the system evolves in just the opposite way. Now the wavelength the system can support increases with time as the forcing is decreased. The pattern needs, thus, to readjust its wavelength and this is done via zigzag instability [38]. As time evolves the forcing reaches the lowest value again and the system readjusts to exhibit a configuration very similar to that in Fig. 1(a) again.

Increasing T ($T = 10\tau$) results in a similar behavior (see Fig. 2). The pattern is forced to evolve from the standard configuration [Fig. 2(a)] to inverted patterns [Figs. 2(b) and 2(c)] and black spots [Fig. 2(d)] right before the pattern is suppressed. As time goes on, the pattern starts recovering. The splitting mechanism plays an important role here again [Fig. 2(g)]. In this case, the stripes do not align perpendicularly to the forcing but they rather choose a direction of 45° [38,39].

For very large values of T ($T = 100\tau$), the centrifugal force varies very slowly and thus the system has enough time to readjust to the changing conditions. This behavior is observed in Fig. 3. Figure 3(a) presents the pattern when the rotational velocity is zero. As time goes on and centrifugal force is increased, the pattern transits into inverted black spots (H_π) that self-organize in a very ordered way [Figs. 3(d) and 3(e)]. Note that in this case, no splitting appears as the changes in the centrifugal forces are so gradual that the pattern has enough time to readjust without any need of splitting mechanisms. Then, the pattern is suppressed [Fig. 3(e)]. Later on, the pattern reappears in the system and stripes appear clearly oriented along the direction of the forcing [Fig. 3(f)]. Zigzag instability occurs [Fig. 3(g)] and the pattern loses the orientation before a new cycle starts again.

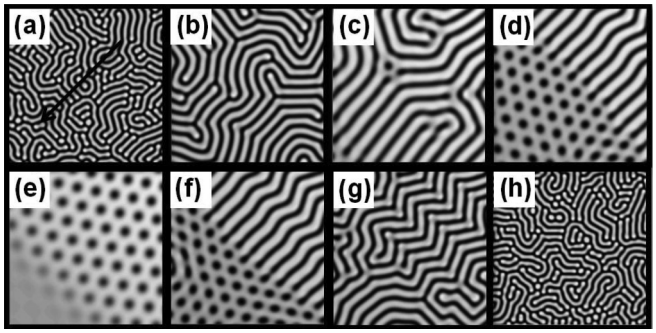

FIG. 3. Effect of the oscillating forcing $\omega(t)$ on Turing pattern formation along a full oscillation for $T \sim 100\tau$. (a–h) correspond to $\omega(t)/\omega_0$: 0, 0.4, 0.6, 0.8, 0.9, 0.7, 0.5, and 0.1, respectively. The direction of the oscillatory force is fixed along the diagonal of the third quadrant [see arrow in (a)] with a maximum value fixed in $\omega_0 = 0.025$ rad/t.u.

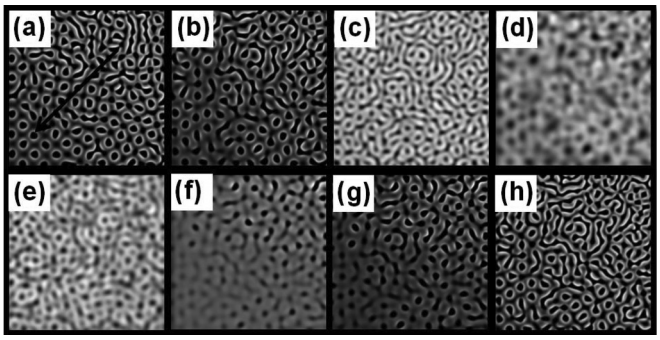

FIG. 4. Black eye pattern. Effect of the oscillating forcing $\omega(t)$ on Turing pattern formation along a full oscillation for $T \sim 0.1\tau$. (a–h) correspond to $\omega(t)/\omega_0$: 0, 0.3, 0.6, 1, 0.7, 0.5, 0.3, and 0, respectively. The direction of the oscillatory force is fixed along the diagonal of the third quadrant [see arrow in (a)] with a maximum value fixed in $\omega_0 = 0.025$ rad/t.u.

Another interesting case occurs at intermediate values of T ($T \sim 0.1\tau$). In this case oscillating black eyes [23,40] appear as described in Fig. 4. For this value of T, the centrifugal force changes very rapidly but the system is still able to see some differences in the force and react accordingly. As a result, the pattern observed is periodically suppressed. Only when centrifugal force is low, the oscillating black eyes pattern arises [see Figs. 4(a) and 4(h)]. Note that the pattern arises almost without transition in the same way as it vanishes.

The behavior of the wavelength with the forcing is analyzed separately. In Fig. 5(a) we present the wavelength variations of the forced pattern with respect to the standard pattern, $\Delta\lambda = \lambda/\lambda_0 - 1$, as a function of time or equivalently the actual value of the rotation frequency ω. Three representative forcing periods are considered: $T \sim 100\tau$, τ, and 0.1τ. The dashed line corresponds with the most probable value of the wavelength as predicted by the theory and following Eq. (5). The shadowed region marks all possible values of the wavelength that are accessible by the system calculated by linear stability analysis [10,32]. These values do not appear spontaneously but if they are imposed by some means they may remain stationary [38].

In the first case, ($T \sim 100\tau$), the pattern adapts so progressively to the centrifugal force that Eckhaus instabilities are not observed. Therefore the wavelength continuously oscillates closely following the theoretical values. In the second case ($T \sim \tau$), the response of the patterns and the period of the forcing are comparable, so changes in the pattern structure are abrupt. It generates a clear wavelength splitting (Eckhaus phenomenon) and two wavelengths coexist while forcing is decreasing (shown as a discontinuity in the line). Note that all the values of the exhibited wavelength are stable for each particular value of ω. In the last case, when the response of the pattern is slow comparing to the period of the forcing patterns, the system exhibits a black eyes arrangement, and we observe splitting at both sides of the maximum wavelength increment. In the latest two cases, the observed wavelengths deviate from the theoretical prediction as the pattern is not able to adapt to the changing conditions; thus other types of instabilities are to happen as described before. Nevertheless, all the values of the wavelength that the system exhibits are compatible, as

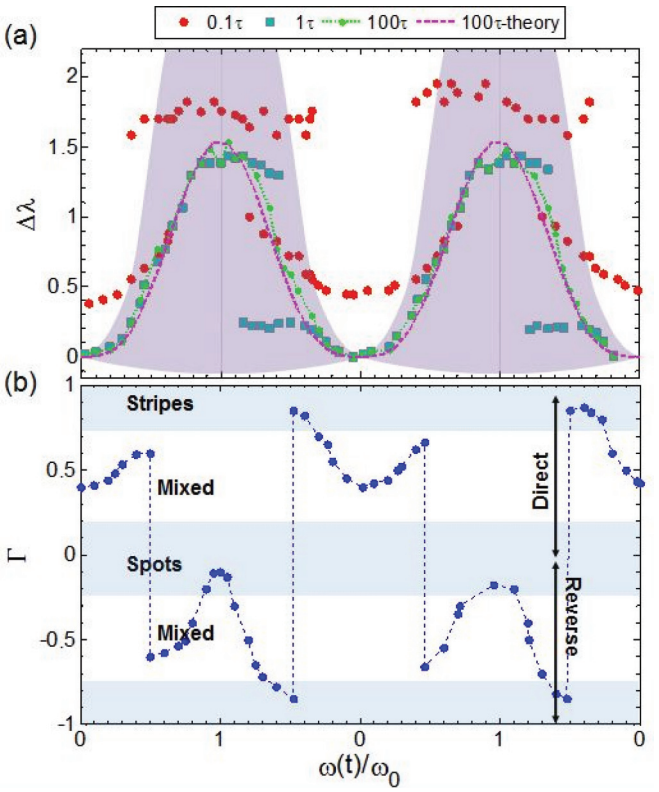

FIG. 5. (Color online) (a) Wavelength increments with respect to the standard pattern, $\Delta\lambda = \lambda/\lambda_0 - 1$, versus forcing. Blue squares, dotted green line, and red circles correspond to the following forcing periods taken from Figs. 1, 3, and 4: $T = \tau$, $T = 100\tau$, and $T = 0.1\tau$, respectively. The shadowed region corresponds to theoretical increments (at $T = 100\tau$) suitable for the Turing regime, with the dashed pink line as the most probable increment. (b) Morphological characterization of Turing patterns with Γ parameter versus forcing (for $T \sim \tau$). $\Gamma = -\alpha\,\mathrm{sign}(E)$, with E the Euler number and α the mean eccentricity of the patterns. All magnitudes in this figure were measured at $\omega_0 = 0.025$ rad/t.u and $R = 1000$ s.u.

a first approximation, with the theoretical Turing conditions and, thus, they are allowed to exist.

This quasisinusoidal behavior of the wavelength is obtained at fixed R; however, in a previous work [32], the wavelength of the patterns under a constant centrifugal field was observed to depend on a semilog law with the distance to the rotation center.

In order to classify the different patterns observed so far, we develop a morphological characterization depending on the applied forcing. This analysis classifies and discriminates by a unique parameter direct from reverse structures, as well as between spots, stripes, or mixed states. An analogous characterization was developed by Mecke *et al.* in [41,42] using Minkowski functionals [43] as morphological measures in order to discriminate between different Turing structures in CDIMA reaction, in porous media or even in galaxies distributions in the universe. We consider here a parameter (Γ) widely tested on the characterization of Turing structures [44]. It is defined by $\Gamma = -\alpha\,\mathrm{sign}(E)$, where α is the mean eccentricity of the patterns distribution and E is the Euler number. The Euler number presents negative or positive values

depending on whether the structures are direct or reversed, respectively. The eccentricity takes a value equal to 0 for pure circular spots (or 1 for straight stripes).

The morphological modifications that the oscillating forcing induces on Turing patterns are shown in Fig. 5(b). Here, Γ parameter is plotted as a function of the forcing for the case of $T \sim \tau$. Low values of forcing from $\omega(t)/\omega_0 = 0$ to 0.5 present positive values of Γ (0.4–0.6, respectively) which indicates the structures are direct. In this region, the structures are formed by a mixed state of spots and stripes that increases the ratio of stripes with the forcing. This tendency is kept until a certain forcing is reached; after that the pattern changes to reverse structures and therefore Γ takes negative values (equal to -0.6). During the interval $\omega(t)/\omega_0 = 0.5$ to 1 this reversed mixed state is gradually transformed into black spots with a value of gamma close to zero ($\Gamma = -0.1$) due to the low eccentricity of the spots.

Then, while the forcing decreases the black spots change to completely orientated stripes by the Eckhaus mechanism at $\omega(t)/\omega_0 = 0.5$ with Γ of -0.9. In addition, the Eckhaus transforms the reversed structure to direct and Γ turns positive. Finally, when the forcing goes on decreasing to zero, the zigzag instability breaks the stripes into a mixed state with a Γ of 0.5.

B. Effect of a strong radial gradient on the oscillatory centrifugal force

The oscillating angular motion has a strong dependence on the radius [see Eq. (4)] and it is reflected on the Turing instability. Figure 6 shows the evolution of the structures for three different values of the rotation period close to the rotation center. Note that now the centrifugal forcing acting on the system is radius dependent and thus the patterns organize and evolve with angular symmetry, including an external ring where the pattern completely disappears as the centrifugal force reaches its maximum.

Similarly to the previous section, low periods of the forcing ($T \sim 0.001\tau$) result in a situation where the patterns just feel the average value of the centrifugal force [Fig. 6(a)]. Note that there is no evolution of the pattern as observed in Figs. 6(a.1)–6(a.4). The picture at the left (SP.A) presents the space-time plot of the points along the line marked SP.A in the figure. Curvature of the lines in this space-time plot indicates an intrinsic motion of the patterns in the direction of the centrifugal force and it will be analyzed in detail below.

The effect of intermediate values of the forcing period ($T \sim \tau$) is shown in Fig. 6(b). Now the structures present an oscillatory behavior. At the maximum forcing [Fig. 6(b.2)] the pattern mainly disappears while at the minimum [Fig. 6(b.4)] the pattern occupies the entire domain with a uniform wavelength. The left panel in Fig. 6(b) shows the space-time plot of line SP.B. The dynamics here reflected are completely different. Despite the oscillatory forcing being a sinusoid the response of the pattern is not symmetric. Firstly, the Eckhaus instability occurs only while the strength of the forcing decreases. Secondly, the pattern undergoes a more abrupt change in its spatial extension while the forcing increases (this is clearly seen in the zoomed area plotted). This is a clear demonstration of the existence of two different temporal scales in the system, one associated with the development of a new pattern and the other associated with the time needed to suppress the pattern.

Figure 6(c) presents the evolution of a pattern when $T \sim 100\tau$. The evolution of the pattern is much faster than the changes in the forcing and so the pattern has enough time to adjust to the changing values of the centrifugal force. For this reason, the pattern in Fig. 6(c.2) presents a radial configuration. In this case, the Eckhaus instability does not play any role and the behavior is symmetric both while increasing the strength of the centrifugal force and while decreasing it (see space-time plot of line SP.C). Note that in this case, the whole pattern also experiences a net displacement in the direction of the centrifugal force.

The space-time plots SP.A and SP.C in Fig. 6 (left column) show an important curvature in the trajectories and this implies that the patterns are forced to move in the direction given by the centrifugal force.

For the patterns shown in Fig. 6(a), with $T \sim 0.001\tau$, the system effectively feels the mean value of the forcing and we observe a displacement of the patterns from the center to the boundary where they disappear with a growing velocity. This phenomenon is similar to the drift of Turing patterns observed in a BZ-AOT system subjected to an electrostatic field [45].

The measure of the drift velocity versus the rotation center is plotted in Fig. 7. When $T \sim 0{,}001\tau$ we obtain a straight line of slope $b_{0.001\tau} = 0.041\,(\text{s.u.})^{-1}$, that is, related to the drift velocity and therefore to the angular velocity. This forcing corresponds to the patterns shown in Fig. 6(a) where the angular velocity is approximately constant. To measure the drift velocity we take an individual pattern path along the space-time plot (SP.A), i.e., from the center to the boundary where patterns disappear. When $T \sim 100\tau$ the angular velocity is time dependent and it is reflected in the nonlinear plot ($b_{100\tau}$ curve). Arbitrarily, we divide the curve in three parts and adjust each one to straight lines of constant slope: $b1_{100\tau} = 0.036\,(\text{s.u.})^{-1}$, $b2_{100\tau} = 0.073\,(\text{s.u.})^{-1}$, and $b3_{100\tau} = 0.153\,(\text{s.u.})^{-1}$. It allows us to compare the drift velocity at different distances from the rotation center. We observe that far from the center (close to the region where the pattern disappears) the slope is almost 4 times higher; it means that the drift velocity and the diffusive transport are maximum in this region.

IV. DISCUSSION AND CONCLUSION

In this paper, we studied numerically the Turing instability in a BZ-AOT system subjected to an oscillatory centrifugal force. This kind of forcing modifies the diffusive transport and therefore the Turing pattern formation is altered, as was reported experimentally in [32]. To consider the effects of the forcing into the Turing pattern formation we included a time-dependent anisotropy in the Oregonator model that results in an effective anisotropic diffusion coefficient. This is a very natural way to introduce a time-dependent anisotropy in a pattern-forming system that actually can be directly extended into experiments as was previously demonstrated [32].

A strong coupling was shown between the period of the oscillating centrifugal force and the characteristic time required by a pattern to develop in the absence of forcing.

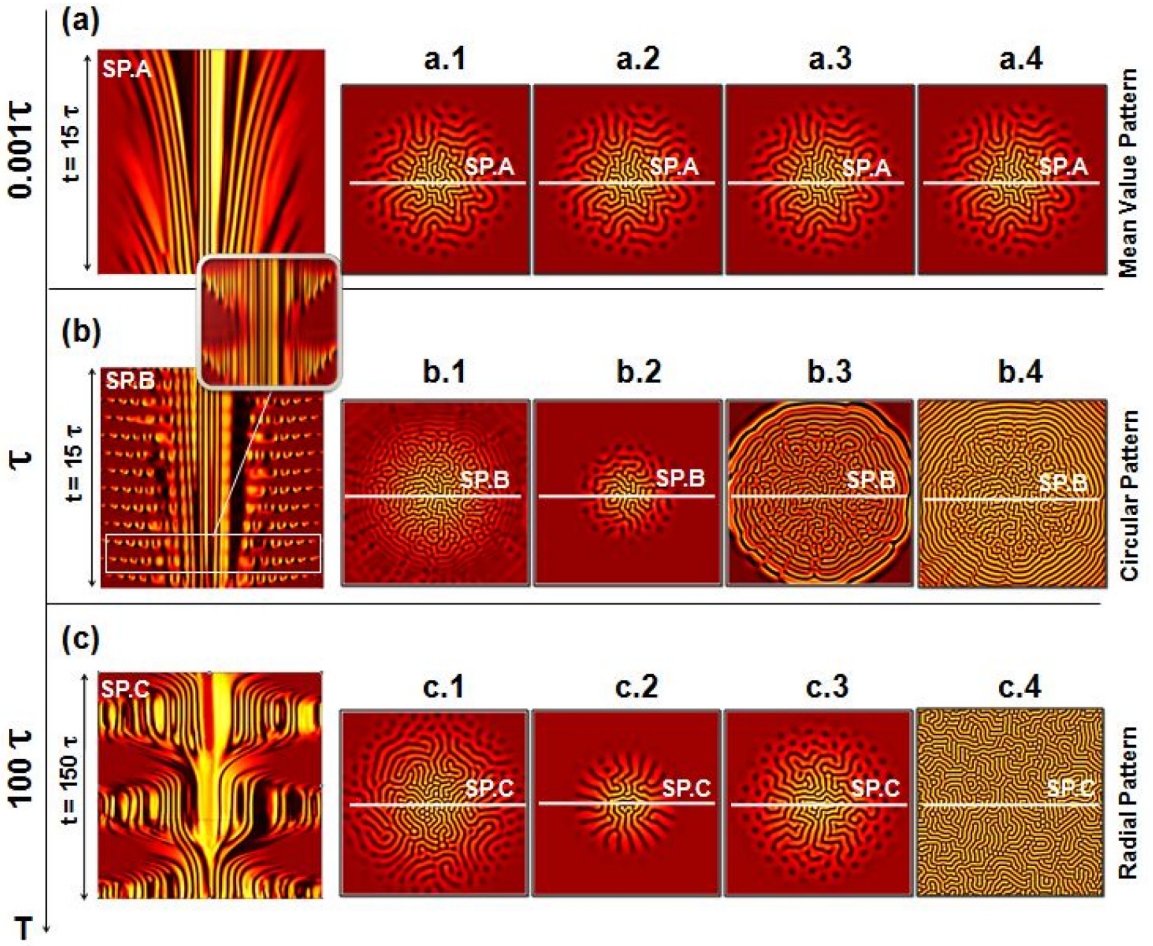

FIG. 6. (Color online) Turing instability coupled to an oscillatory centrifugal force close to the rotation center. The computational domain consists of a two-dimensional mesh of 300 × 300 grid points, with a spatial step of 0.2 s.u. Three sequences of snapshots were taken for three different oscillation periods (a–c) at different forcings along a full oscillation, i.e., $\omega(t)/\omega_0 = 0.5, 1.0, 0.5,$ and 0, denoted as 1, 2, 3, and 4, respectively. The magnitude of the forcing remains at $\omega_0 = 0.40$ rad/t.u. (a) Oscillation period $T = 0.001\tau$. SP.A is the space-time plot of the mean value pattern showed in (a.1)–(a.4) for an interval of $(t = 15\tau)$. (b) Oscillation period $T = \tau$. SP.B is the space-time plot of the circular patterns shown in (b.1)–(b.4) for an interval of $(t = 15\tau)$. The zoom corresponds to an interval of 2τ. (c) Oscillation period $T = 100\tau$. SP.C is the space-time plot of the radial pattern showed in (c.1)–(c.4) for an interval of $(t = 150\tau)$.

The configurations presented by Turing structures are different depending on the magnitude and the period of the forcing. In fact, a wide range of different static and nonstatic patterns were described, as well as the different instabilities that eventually yield to the patterns.

The dependence of the orientation of the stripes pattern with the chosen frequency is noteworthy [see Figs. (1)–(3)]. Low periods imply that the boundary where patterns disappear moves relatively fast compared with the growth velocity for the pattern. Thus the pattern grows parallel to that boundary. For high values of the period, the boundary where patterns disappear moves very slowly and the pattern is forced to grow with the boundary; thus it grows in the axial direction. Intermediate values of the period result in a mixed state of stripes oriented in an oblique direction. This is formally equivalent to the case described in [33].

The other patterns that appear are related with the mechanism to adapt to the changing wavelength in the medium. For large periods the wavelength of the structure naturally fits with the theoretically expected values. For the other cases, there are several such mechanisms and the particular election of the mechanism is usually determined by the velocity of the change and the direction of the change (whether it increases or decreases), as well as on the particular values of the model parameters (whether there are subcritical patterns that may become temporally more stable, etc.). Some detailed analysis of such transitions can be found in [38]. It is important to remark here that independently of the particular mechanism chosen by the system to adapt its wavelength to the changing conditions, the exhibited wavelength is always compatible with the Turing conditions.

Another important observation from the results presented here is the existence of two different temporal scales in the system that resulted in some sort of hysteresis phenomenon discussed in Figs. 5(a) and 6(b). We observed that depending on whether the forcing is increasing or decreasing, the response of the patterns was different, as revealed by the wavelength analysis in Fig. 5(a) and the space-time plots in Fig. 6(b). The hysteresis phenomenon on Turing patterns was observed in networks [46], but chemical systems such as

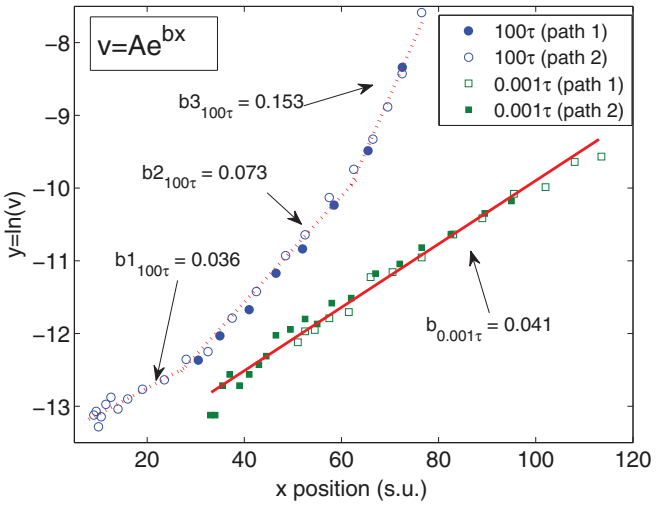

FIG. 7. (Color online) Semilog plot of the drift velocity [ln(v), with ln as the natural log] for the Turing patterns subjected to the oscillating angular motion versus the position with respect to the rotation center (x). The velocity was measured from the space-time plots (SP.A and SP.C) of Fig. 6. Circles (squares) correspond to the patterns subject to a period of forcing of $T = 0.001\tau$ ($T = 100\tau$). Paths 1 and 2 indicate the trajectories of any two patterns from the center to the disappearance region.

BZ-AOT need more study. At enough high periods, hysteresis disappears and patterns are able to take the sense of the centrifugal force presenting a radial arrangement. In addition, the space-time analyses stated that each individual pattern underwent an intrinsic motion in the sense of the centrifugal force.

In this paper we exploited the experimental result that anisotropy can be induced in a system by external means. By modulating the external forcing, centrifugal force in this case, we were able to induce time-dependent anisotropies in the system and analyze their effects on pattern formation. A large variety of patterns was reported here endowed with complicated dynamics. This work will aid future research as it describes the possibility to dynamically change properties of the active medium that, otherwise, are constant and noncontrollable.

ACKNOWLEDGMENTS

This work was supported by Xunta de Galicia under Research Grant No. CN2012/315. J.G.-S. was supported by the Xunta de Galicia under a Predoctoral Grant.

[1] D. G. Míguez, E. M. Nicola, A. P. Muñuzuri, J. Casademunt, F. Sagués, and L. Kramer, Phys. Rev. Lett. **93**, 048303 (2004).
[2] A. P. Muñuzuri, M. Dolnik, A. M. Zhabotinsky, and I. R. Epstein, J. Am. Chem. Soc. **121**, 8065 (1999).
[3] V. K. Vanag and I. R. Epstein, Proc. Natl. Acad. Sci. U.S.A. **100**, 14635 (2003).
[4] J. Guiu-Souto, J. Carballido-Landeira, V. Perez-Villar, and A. P. Muñuzuri, Phys. Rev. E **82**, 066209 (2010).
[5] L. Yang and I. R. Epstein, Phys. Rev. Lett. **90**, 178303 (2003).
[6] A. M. Turing, Philos. Trans. R. Soc., B **237**, 37 (1952).
[7] J. Reinitz, Nature **482**, 464 (2012).
[8] K. J. Painter, P. K. Maini, and H. M. Othmer, Proc. Natl. Acad. Sci. U.S.A. **96**, 5549 (1999).
[9] M. Kærn, M. Menzinger, R. Satnoianu, and A. Hunding, Faraday Discuss. **120**, 295 (2002).
[10] J. D. Murray, *Mathematical Biology II: Spatial Models and Biomedical Applications* (Springer, Berlin, 2003).
[11] S. Sawai, Y. Maeda, and Y. Sawada, Phys. Rev. Lett. **85**, 2212 (2000).
[12] J. B. L. Bard, J. Theor. Biol. **93**, 363 (1981).
[13] S. Kondo and R. Asai, Nature **376**, 765 (1995).
[14] J. H. E. Cartwright, J. Theor. Biol. **217**, 97 (2002).
[15] V. Castets, E. Dulos, J. Boissonade, and P. De Kepper, Phys. Rev. Lett. **64**, 2953 (1990).
[16] Q. Ouyang and H. L. Swinney, Nature **352**, 610 (1991).
[17] A. J. Chaplain, G. D. Singh, and J. C. McLachlan, *On Growth and Form: Spatiotemporal Pattern Formation in Biology* (John Wiley & Sons, Chichester, 1999).
[18] I. K. Quigley and D. M. Parichy, Microsc. Res. Tech. **58**, 442 (2002).
[19] J. Carballido-Landeira, V. K. Vanag, and I. R. Epstein, Phys. Chem. Chem. Phys. **12**, 3656 (2010).
[20] E. Dulos, P. Davies, B. Rudovics, and P. De Kepper, Physica D (Amsterdam, Neth.) **98**, 53 (1996).
[21] D. G. Míguez, S. Alonso, A. P. Muñuzuri, and F. Sagués, Phys. Rev. Lett. **97**, 178301 (2006).
[22] G. H. Gunaratne, D. K. Hoffman, and D. J. Kouri, Phys. Rev. E **57**, 5146 (1998).
[23] G. H. Gunaratne, Q. Ouyang, and H. L. Swinney, Phys. Rev. E **50**, 2802 (1994).
[24] A. Kaminaga, V. K. Vanag, and I. R. Epstein, J. Chem. Phys. **122**, 174706 (2005).
[25] V. Dufiet and J. Boissonade, Physica A (Amsterdam, Neth.) **188**, 158 (1992)
[26] I. Berenstein and A. P. Muñuzuri, J. Chem. Phys. **129**, 114508 (2008).
[27] A. Kaminaga, V. K. Vanag, and I. R. Epstein, Angew. Chem., Int. Ed. **45**, 3087 (2006).
[28] B. P. Belousov, in *Collected Abstracts on Radiation Medicine*, edited by A. V. Lebedinskii (Medgiz, Moscow, 1959).
[29] A. N. Zaikin and A. M. Zhabotinsky, Nature **225**, 535 (1970).
[30] V. K. Vanag, Phys. Usp. **47**, 923 (2004).
[31] V. K. Vanag and I. R. Epstein, Phys. Rev. Lett. **87**, 228301 (2001).
[32] J. Guiu-Souto, L. Michaels, A. von Kamenke, J. Carballido-Landeira, and A. P. Muñuzuri, Soft Matter **9**, 4509 (2013).
[33] D. G. Míguez, M. Dolnik, A. P. Muñuzuri, and L. Kramer, Phys. Rev. Lett. **96**, 048304 (2006).
[34] A. K. Horváth, M. Dolnik, A. P. Muñuzuri, A. M. Zhabotinsky, and I. R. Epstein, Phys. Rev. Lett. **83**, 2950 (1999).

[35] L. Gyorgyi, T. Turanyi, and R. J. Field, J. Phys. Chem. **94**, 7162 (1990).
[36] K. Huang, *Statistical Mechanics*, 2nd ed. (John Wiley & Sons, New York, 1987).
[37] F. A. William, *Numerical Methods for Partial Differential Equations* (Academic Press, New York, 1977).
[38] B. Peña, C. Pérez-García, A. Sanz-Anchelergues, D. G. Míguez, and A. P. Muñuzuri, Phys. Rev. E **68**, 056206 (2003).
[39] D. G. Míguez and A. P. Muñuzuri, Biophys. Chem. **124**, 161 (2006).
[40] L. Yang, M. Dolnik, A. M. Zhabotinsky, and I. R. Epstein, Phys. Rev. Lett. **88**, 208303 (2002).
[41] K. R. Mecke, Phys. Rev. E **53**, 4794 (1996).
[42] K. R. Mecke, T. Buchert, and H. Wagner, Astron. Astrophys. **288**, 697 (1994).
[43] H. Minkowski, Math. Ann. **57**, 447 (1903); *Theorie der konvexen Körper, insbesondere Begründung ihres Oberflächenbegriffs*, Vol. 2 (Gesammelte Abhandlungen, Leipzig, 1911).
[44] J. Guiu-Souto, J. Carballido-Landeira, and A. P. Muñuzuri, Phys. Rev. E **85**, 056205 (2012).
[45] J. Carballido-Landeira, P. Taboada, and A. P. Muñuruzi, Soft Matter **8**, 2945 (2012).
[46] H. Nakao and A. S. Mikhailov, Nat. Phys. **6**, 544 (2010).